



HAL
open science

Role of grain boundaries in the diffusion of hydrogen in nickel base alloy 600: Study coupling thermal desorption mass spectroscopy with numerical simulation

Caitlin Hurley, Frantz Martin, Loic Marchetti, Jacques Chêne, Christine Blanc, Eric Andrieu

► To cite this version:

Caitlin Hurley, Frantz Martin, Loic Marchetti, Jacques Chêne, Christine Blanc, et al.. Role of grain boundaries in the diffusion of hydrogen in nickel base alloy 600: Study coupling thermal desorption mass spectroscopy with numerical simulation. *International Journal of Hydrogen Energy*, 2016, 41 (38), pp.17145-17153. 10.1016/j.ijhydene.2016.07.038 . hal-01567014

HAL Id: hal-01567014

<https://hal.science/hal-01567014>

Submitted on 21 Jul 2017

HAL is a multi-disciplinary open access archive for the deposit and dissemination of scientific research documents, whether they are published or not. The documents may come from teaching and research institutions in France or abroad, or from public or private research centers.

L'archive ouverte pluridisciplinaire **HAL**, est destinée au dépôt et à la diffusion de documents scientifiques de niveau recherche, publiés ou non, émanant des établissements d'enseignement et de recherche français ou étrangers, des laboratoires publics ou privés.



Open Archive TOULOUSE Archive Ouverte (OATAO)

OATAO is an open access repository that collects the work of Toulouse researchers and makes it freely available over the web where possible.

This is an author-deposited version published in : <http://oatao.univ-toulouse.fr/>
Eprints ID : 18102

To link to this article : DOI:10.1016/j.ijhydene.2016.07.038
URL : <http://dx.doi.org/10.1016/j.ijhydene.2016.07.038>

To cite this version : Hurley, Caitlin and Martin, Frantz and Marchetti, Loïc and Chêne, Jacques and Blanc, Christine and Andrieu, Eric *Role of grain boundaries in the diffusion of hydrogen in nickel base alloy 600: Study coupling thermal desorption mass spectroscopy with numerical simulation.* (2016) International Journal of Hydrogen Energy, vol. 41 (n° 38). pp. 17145-17153. ISSN 0360-319

Any correspondence concerning this service should be sent to the repository administrator: staff-oatao@listes-diff.inp-toulouse.fr

Role of grain boundaries in the diffusion of hydrogen in nickel base alloy 600: Study coupling thermal desorption mass spectroscopy with numerical simulation

Caitlin Hurley ^{a,b,*}, Frantz Martin ^a, Loïc Marchetti ^{a,c}, Jacques Chêne ^d, Christine Blanc ^b, Eric Andrieu ^b

^a CEA, DEN, DPC, SCCME, Laboratoire d'Étude de la Corrosion Aqueuse, 91191, Gif-sur-Yvette, France

^b Université de Toulouse, Institut Carnot CIRIMAT, UPS/INPT/CNRS, ENSIACET, 4 allée Emile Monso, 31030, Toulouse Cedex 4, France

^c CEA, DEN, MAR, DTCD, SECM, Laboratoire d'Études du Comportement à Long Terme de matériaux de conditionnement, 30207, Bagnols sur Cèze, France

^d CNRS/CEA UMR 8587, CEA Saclay, 91191, Gif-sur-Yvette, France

ABSTRACT

The role grain boundaries play in the diffusion of hydrogen in polycrystalline alloys has long been debated. Some researchers have found that grain boundaries have an accelerating effect on the transport of hydrogen across a metal membrane, while others have stated this network of sites may slow the diffusion of hydrogen or have a mixed effect depending on grain size and orientation. Thermal desorption mass spectroscopy (TDS) was used to study the diffusion of deuterium, from 294 K to 550 K, in model single crystal and polycrystalline nickel base alloy, alloy 600, having a grain size of several tens of micrometers. Using a numerical routine, solving Fick's second law of diffusion, TDS spectra were fit or simulated. The derived diffusion constant parameters ($D_0 = (1.0 \pm 0.5) \cdot 10^{-2} \text{ cm}^2 \text{ s}^{-1}$ and $E_D = (45 \pm 4) \text{ kJ mol}^{-1}$) for the polycrystalline alloy adequately predict and simulate the deuterium desorption from the single crystal during TDS testing. Furthermore, in the temperature range and for the grain size studied no significant effect of grain boundaries on the diffusion of deuterium in alloy 600 was observed. Consequently, the measured diffusion parameters are representative of interstitial diffusion in the alloy.

Keywords:

Deuterium
Diffusion
Hydrogen
Grain boundaries
Ni base alloy
Thermal desorption mass spectroscopy

Introduction

For over five decades researchers have observed the cracking of nickel base alloy 600 (A600) during exposure to high

temperature water environments [1,2]. This alloy, which normally presents good corrosion resistance, is often used as the structural material of the Steam Generator (SG) tubes found in Pressurized Water Reactor (PWR) nuclear power plants. These tubes serve as the barrier between the primary

* Corresponding author. VTT Technical Research Centre of Finland Ltd., Nuclear Reactor Materials, P.O. Box 1000, 02044 VTT, Finland.
E-mail address: caitlin.hurley@vtt.fi (C. Hurley).
<http://dx.doi.org/10.1016/j.ijhydene.2016.07.038>

(high temperature, high pressure aqueous medium, hydrogen gas overpressure (25–50 cm³ kg⁻¹ NPT)) and secondary circuits (saturated steam).

The cracking of these tubes has since been referred to as Stress Corrosion Cracking (SCC) and the role hydrogen (H) may play in this phenomenon has been explored [3–10]. Numerous researchers have stated that H may affect the material's sensitivity to this type of degradation and furthermore affect the initiation and propagation of these cracks. Among the roles hydrogen may play in SCC, an effect on the local mechanical properties of the alloy was proposed in literature [5,11–13]. Before H can play this type of role in SCC phenomenon, it must first be absorbed by the material. After absorption, the hydrogen will be transported across the alloy. As a general approach, this process can be described by Fick's second law of diffusion:

$$\frac{\partial c_H}{\partial t} = D \frac{\partial^2 c_H}{\partial x^2} \quad (1)$$

where c_H , t , D , and x represent respectively the local molar fraction of hydrogen, time, the interstitial diffusion coefficient, and position in the material.

However, during the diffusion process occurring in “real” alloys, the hydrogen atoms will interact with both (i) interstitial lattice sites and (ii) crystallographic heterogeneities intrinsically present in the material (i.e. vacancies, dislocations, grain boundaries, etc.). There is a large debate surrounding the nature of these sites and the possible effect they may have on the H transport process. These sites could “trap” H and therefore have a relative slowing effect on its [apparent] diffusion coefficient or even act as “short-circuits”, especially along grain boundaries (GB), and therefore enhance the relative transport of hydrogen across the metal.

While most researchers consider the nature of some sites, such as precipitate interfaces, to be identified as traps sites (TS) for hydrogen (for example chromium carbides are considered to be trap sites) [14,15], the role of some sites or networks of sites, such as grain boundaries, is not so clear. Experimental and numerical studies have resulted in mixed results in both pure and alloyed materials. Some researchers have observed a short-circuit effect of grain boundaries [16–22], whereas others have noted a trapping effect [23,24] and again others reporting a “mixed” effect dependent on numerous material parameters (i.e. grain size [21], number of triple junctions [25], Geometrically Necessary Dislocations (GND) [25] and/or GB orientation [26]). Based upon these very mixed findings, it would seem that this subject needs to be handled on a material-to-material (i.e. depending on chemical composition, microstructure, etc.) basis and looking at the effect GBs may have on H transport in the concerned material before drawing any conclusions on the H-material interactions.

In the body of this article, the role grain boundaries play in H diffusion and/or trapping in nickel base alloy 600, having a grain size of several tens of micrometers, will be discussed. The diffusion of hydrogen and its isotopes (deuterium (²H) and tritium (³H)) in A600 has been studied in previous works in the temperature range of 423 K–675 K [27] and 573 K–973 K [28]. The D_0 and E_D values obtained in these two studies for H, ²H and ³H are relatively close; this seems to demonstrate that the

isotopic effect is negligible with regards to the uncertainty associated with the measurement and determination of the diffusion coefficient. Unfortunately, grain size was not specified in either publication [27,28] and therefore it is impossible to evaluate the effect of grain boundaries based solely upon these previous works.

As to better address the role of grain boundaries on the diffusion of hydrogen, the transport of an isotopic hydrogen tracer, deuterium (²H) will be experimentally assessed in polycrystalline A600 and A600-like single crystal specimens by thermal desorption mass spectroscopy (TDS). These results will then be analyzed using the numerical simulation of Fick's second law of diffusion, Eq. (1), and spectral fitting approach described in a previous article [29]. Using this coupled experimental and numerical approach the deuterium diffusion coefficient in A600 was determined and the role grain boundaries may play in the H diffusion phenomenon in this specific material is addressed.

Materials and method

Model materials and sample preparation

As the objective of this paper was to address the role of grain boundaries in the H diffusion process, it was necessary to work with (i) a model material containing [almost] only grain boundaries, as heterogeneities liable to interact with H, and (ii) a model material free of grain boundaries, in which H transport is governed by interstitial diffusion. Therefore, two materials were chosen: (i) a polycrystalline nickel base alloy 600 (A600-pc) and (ii) a single crystal¹ (A600-sc) with a chemical composition close to that of the polycrystalline alloy, see Table 1.

Polycrystalline A600

Material observations were carried out on the as-received material. This highlighted the presence of inter- and intragranular chromium carbides, identified as Cr₇C₃, and some titanium carbonitrides (TiCN) in the industrial (as-received) A600 (respectively the smaller and larger black forms in Fig. 1a) along with an inhomogeneous grain structure characterized by bands of small (55 ± 7 μm) and large (120 ± 5 μm) grains.

To eliminate the large majority of precipitates and the residual cold working from the polycrystalline material, the as-received A600 slabs were treated in a similar way to [30]. First, the slabs were maintained at 1453 K for 1 h under vacuum then rapidly quenched in water. This thermal treatment aimed at eliminating the residual cold working and solutionizing the majority of chromium carbide precipitates. Following this treatment the slabs were tempered at 573 K for 15 h and slow air cooling in order to eliminate the thermal vacancies possibly retained in the material during the quench. The resulting microstructure can be seen in Fig. 1b and c.

These heat treatments resulted in successful elimination of chromium carbides as well as the large majority of

¹ Provided by the Ecole Nationale Supérieure des Mines de Saint-Etienne, France.

Table 1 – Chemical composition (wt.%) of the polycrystalline Ni-base alloy 600 (A600-pc) and of the A600-like single crystal (A600-sc) studied.

Element	C	Mn	Si	S	P	Ni	Cr	Cu	Co	Fe	Ti	Al
A600-pc	0.06	0.82	0.31	<0.001	0.008	base	15.8	0.01	0.01	9.6	0.196	0.164
A600-sc	n.s. ^a	0.01	0.08	0.01	0.01	base	16.99	0.02	0.01	5.57	<0.01	–

^a Non-specified.

dislocations. After analyzing several images obtained by transmission electron microscopy (TEM), example in Fig. 1c, the average residual dislocation density was evaluated as $(3.6 \pm 0.1) \cdot 10^8 \text{ cm}^{-2}$ which may be considered fairly low. Regarding the grain size, scanning electron microscopy (SEM) and optical microscopy (OM) (images not shown) have revealed that the banded grain structure, while being less pronounced, was still present after thermal treatments. Larger and smaller grains were on the order of $127 \pm 9 \mu\text{m}$ and $68 \pm 9 \mu\text{m}$ respectively. The thermal treatments did not result in the elimination of the TiCNs, indicated by the white arrows

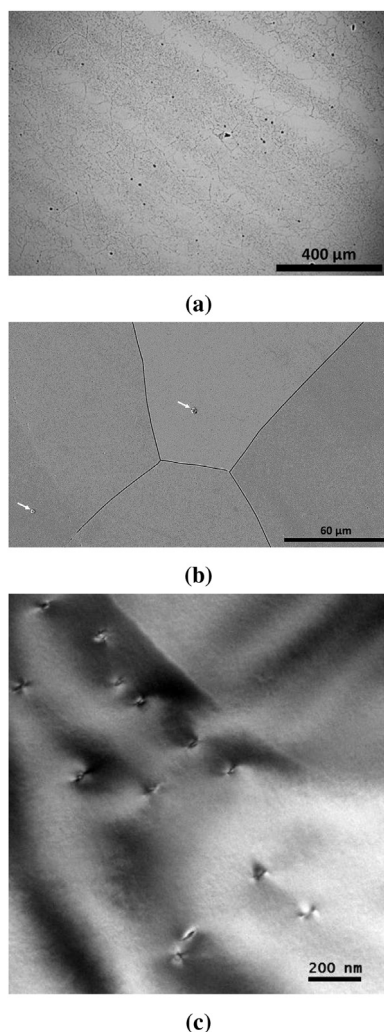


Fig. 1 – Observations of the A600-pc in its (a) as-received state by OM and its heat treated state by (b) SEM and (c) TEM. The white arrows in (b) indicate the TiCN which were not eliminated by the series of thermal treatments.

in Fig. 1b. Nevertheless, considering that (i) very few of these precipitates were present and (ii) the residual dislocation density is very low, the possible effects of these heterogeneities on the diffusion (and trapping) of hydrogen in this material can be supposed negligible. Therefore, all H-material interactions taking place in this “model” (i.e. heat treated) polycrystalline A600 specimens may be attributed to interstitial and/or grain boundary diffusion.

A600-like single crystal

The microstructure of the A600-like single crystal (A600-sc) was observed microscopically. This revealed a homogeneous material with no observable grain boundaries nor precipitations (i.e. chromium carbides or TiCN) even after TDS testing.

Sample preparation

The A600-pc and A600-sc slabs were then sectioned into smaller samples measuring $1.3 \text{ cm} \times 1.3 \text{ cm}$ with a $0.3 \text{ cm} \times 0.5 \text{ cm}$ tab and a starting thickness of 0.11 cm by electrical discharge machining. Sample edges were first ground down to 1200 grit SiC paper, then both sample faces were mechanically polished from SiC 800 grit paper down to a mirror finish using a $0.04 \mu\text{m}$ aluminum oxide colloidal suspension, with a final preparation step of 2 h on a vibrating table in the suspension.

This finishing step minimized the surface cold working induced during the mechanical polishing process, see Fig. 2. While the single crystal model material is softer on the surface, as compared to the polycrystalline model material, the “core” hardness is very similar. After surface preparation, sample thickness ranged from 0.07 cm to 0.09 cm and the width remained nearly unchanged; the final dimensions of each sample were carefully recorded.

Cathodic deuterium charging

Deuterium (^2H) is used as an isotopic tracer for hydrogen and has been shown to result in a much more stable and unpolluted signal when using the TDS experimental technique which will be presented in more detail in the next subsection. Before charging, a thin copper wire was welded by resistive spot welding to the specimen tab. Only one sample face was left exposed to the solution; the rest, including the Cu wire and tab, was protected from solution exposure by a Lacomite™ varnish.

Deuterium (^2H) was introduced into the sample by cathodic charging in a deaerated (Ar bubbling) $^2\text{H}_2\text{O}$ (99.90% ^2H) solution containing 0.1 M NaOH by applying a cathodic current (-100 mA cm^{-2}) for 30 min at 298 K. After charging, the Lacomite™ varnish and tab with attached Cu wire is removed leaving the square sample. Specimen are then either

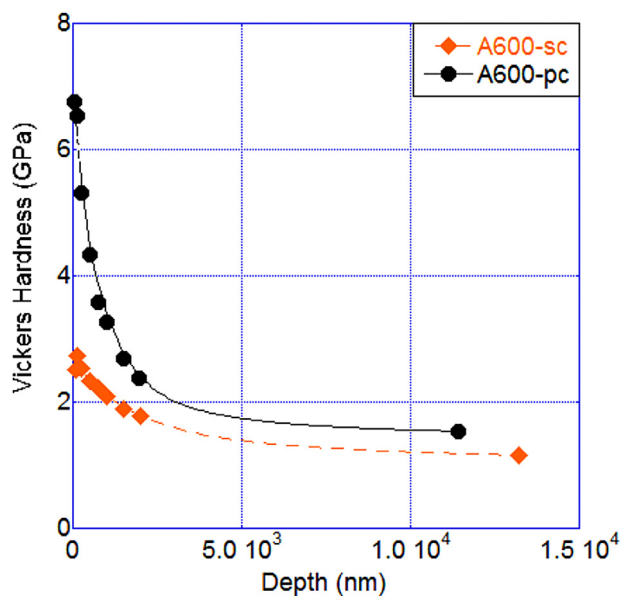


Fig. 2 – Nano- and microindentation results for the model A600-pc and A600-sc after mechanical polishing and 2 h on the vibrating table in an aluminum oxide colloidal suspension.

transferred directly to the TDS set-up or are quickly stored in liquid nitrogen for testing at a later date. This transfer time is duly noted and taken into consideration in experimental analysis [29].

Experimental method and data analysis

This study used an approach which coupled experimental thermal desorption mass spectroscopy analysis with a numerical simulation code to both fit or simulate experimental results.

Thermal desorption mass spectroscopy

TDS was used to study the H-material interactions taking place in both the A600-pc and A600-sc model materials. This analysis method consisted of subjecting a deuterated specimen to either an isotherm or a temperature ramp under dynamic vacuum while the $^2\text{H}_2$ ionizing current, which is proportional to the desorption flux of $^2\text{H}_2$ molecules from the sample, was continuously monitored in function of time and temperature.

A pre-charged sample was transferred from the cathodic charging set-up to the TDS experimental set-up where it was

placed in a quartz tube which runs through a programmable circular furnace. A type-K thermocouple was located in the furnace very close to the specimen, to monitor the temperature at the sample. When the specimen was inserted into the system, an incompressible pump down time (from atmospheric pressure to the adequate vacuum for mass spectrometer operation) of 15 ± 3 min induced a short room temperature aging of the specimen during which there was no desorption monitoring. This transfer period was also taken into consideration in numerical analysis [29].

Two types of TDS analysis were undertaken: (i) “traditional” TDS analysis, which involved imposing a linear temperature ramp on the system or (ii) “hybrid” TDS analysis. Experimental conditions for these two types of analysis can be seen in Table 2. The hybrid technique involves subjecting the specimen to a prolonged isothermal aging period, at a desired temperature, followed by traditional TDS analysis, i.e. applied dynamic temperature ramp. During both types of analysis the desorption flux was monitored along with the sample temperature. The real temperature ramp applied to the sample was considered in numerical analysis [29].

Two hybrid testing experimental conditions were imposed: (i) a room temperature (294 ± 2 K) aging as low temperatures are often thought to favor short-circuit diffusion along the grain boundary network [20] and (ii) an elevated temperature (409 ± 1 K) aging period which, while grain boundaries may still play a short circuit role at this temperature [22], approaches the temperature range where diffusion in volume is often considered more dominant [31].

Numerical analysis

The resulting experimental TDS spectra were then analyzed using a numerical code developed and presented in a previous article [29]. At the present time, this code can only be used to perform one-dimensional (1D) calculations. This decrease in dimension of the modeled system (1D), compared to that of the real system (3D), is expected to have no significant impact on calculation results, because the thickness of samples used in this study remains very small compared to their length and width (see Section Sample preparation). The system can then be considered finite in one direction and infinite in the two others.

The system could be defined using three different limiting cases (assuming grain boundaries play different roles in the diffusion process).

1. The most simple assuming the system can be described by Fick's second law (Eq. (1)), therefore making the assumptions that:

Table 2 – Experimental conditions for “traditional” and “hybrid” TDS analysis. In this table t_i and T_i (i referring to either “charging”, “transfer” or “aging”) are the duration and temperature of each experimental step and ϕ is the imposed TDS temperature ramp rate.

Analysis type	Charging		Transfer		Aging		T ramp
	t_{charging} (min)	T_{charging} (K)	t_{transfer} (min)	T_{transfer} (K)	t_{aging} (min)	T_{aging} (K)	ϕ (K min^{-1})
Traditional	30	298	15 ± 3	294 ± 2	–	–	10
Hybrid-294 K	30	298	15 ± 3	294 ± 2	360	294 ± 2	10
Hybrid-409 K	30	298	15 ± 3	294 ± 2	360	409 ± 1	10

Table 3 – Pre-exponential constant (D_0) and activation energy (E_D) for the diffusion of ^1H and its isotopic tracers (i.e. ^2H and ^3H) in A600 extracted from literature [27,28] and measured in this study.

	D_0 (cm ² .s ⁻¹)	E_D (kJ mol ⁻¹)
^1H [27]	$1.7 \cdot 10^{-2}$	49.8
^2H [27]	$2.0 \cdot 10^{-2}$	51.9
^3H [28]	$(1.3 \pm 0.5) 10^{-2}$	50.6 ± 2.0
^2H This study	$(1.0 \pm 0.5) 10^{-2}$	45 ± 4

- (a) the diffusion coefficient (D) is considered to follow an Arrhenius relationship (see Eq. (2)), depending on a pre-exponential constant (D_0), activation energy (E_D), the ideal gas constant (R) and temperature (T), the latter giving D its temperature dependence:

$$D = D_0 \times \exp\left(\frac{-E_D}{RT}\right) \quad (2)$$

and

- (b) the ^2H diffusion along grain boundaries can be neglected compared to the ^2H flux resulting from interstitial diffusion in the grain volume.
2. A system where grain boundaries play the role of ^2H diffusion short circuits. Therefore the diffusion coefficient along the grain boundary, D_{GB} , must be considered through the use of an effective diffusion coefficient [31] in Eq. (1) or by a more realistic mathematical description of diffusion in grain boundaries [32,33].
 3. A system where grain boundaries act as potential trap sites for hydrogen. The system could be adapted through the addition of a trap site density, N (expressed here as a molar fraction), and trap site occupancy term would be needed. Therefore simulation and fitting could be made possible by the McNabb and Foster equations (Eq. (3)) [34]:

$$\frac{\partial c_{\text{H}}}{\partial t} + N \frac{\partial \theta_{\text{GB}}}{\partial t} = D \frac{\partial^2 c_{\text{H}}}{\partial x^2} \quad (3a)$$

$$\frac{\partial \theta_{\text{GB}}}{\partial t} = c_{\text{H}} k (1 - \theta_{\text{GB}}) - p \theta_{\text{GB}} \quad (3b)$$

where θ_{GB} represents the fraction of occupied TS (grain boundaries in this case), k the trapping kinetic constant and p the detrapping kinetic constant at grain boundaries.

Systems 2 and 3 require the determination of many temperature dependent parameters such as, for 2., a grain boundary segregation factor (s) or, for 3., the determination or assumption of kinetic trapping and detrapping constants (k and p) and a trap site density (N) at grain boundaries. Considering (i) that it is not realistic to determine a plethora of parameters from a limited amount of experimental results and (ii) that the parameters mentioned above are not readily available in literature, the numerical analysis of experimental results will be attempted using the first system. The validity of this choice will be discussed based upon the comparison of results obtained on single crystal and polycrystalline samples.

On top of assumptions (1a) and (1b), additional assumptions, regarding initial and boundary conditions, are needed to numerically solve Eq. (1):

- (1c) the sample is free of ^2H before cathodic charging,
- (1d) a constant ^2H surface concentration ($c_{0, \text{charging}}$) is imposed at the sample face exposed to the solution during the charging step, whereas
- (1e) the ^2H surface concentration at the varnished face remains equal to zero.

The applicability of hypothesis (1d) has been verified by chronopotentiometry measurements for the entire charging duration as detailed in Ref. [35]. It has been observed for this work that the measured potential remains quasi-constant during the cathodic charging and tends to become independent of time. Such evolution of the potential for a constant imposed current shows that the steady state approximation can be applied to the ^2H surface discharge mechanism, leading to the assumption that the ^2H surface concentration remains constant during charging. The hypothesis (1e) is supported by estimating the ^2H characteristic diffusion length for the charging duration (on the basis of published diffusion data for H (and its isotopes) in A600 [27,28]), which remains small, compared to the sample thickness.

Moreover, the numerical procedure takes into consideration the entire specimen history: (i) duration and temperature of the charging, transfer and aging (if the specimen was subjected to a prolonged aging period) steps and (ii) the experimental temperature ramp imposed to the sample during TDS analysis. This implies to define initial conditions for each step, which are detailed in Ref. [29]. Concerning the associated boundary conditions, as the sample is mainly exposed to a dynamic vacuum during transfer, aging and TDS steps, it is assumed that ^2H surface concentration for both sample faces remains constant and equal to zero during this three steps [29].

Using this set of assumptions, the numerical code was used to determine the pre-exponential constant and activation energy associated with the diffusion coefficient through the fit of “traditional” TDS spectra. This fit uses a numerical routine constructed in Python™. This Python code uses the curve fit function (`scipy.optimize.curve_fit`) which uses the Levenberg–Marquardt algorithm for least squares curve fitting [36]. The developed numerical code can also be used for simulation purposes when the fitting of parameters is not necessary. This is, for example, the case when the use of the code aims to validate previously determined parameters (as discussed in Section [Diffusion coefficient validation](#)). In this last case, an experimental TDS spectrum is compared to its simulated counterpart, the latter based on parameters determined from the fit of another experimental TDS results.

Results and discussion

Experimental results

“Traditional” and “hybrid” TDS desorption spectra were acquired for both the [heat treated] polycrystalline and single

crystal A600 materials, respectively A600-pc and A600-sc. All specimen were precharged with ^2H (30 min at 298 K) before transferring them to the TDS experimental set-up. The applied experimental conditions can be seen in Table 2. The experimental spectra for A600-pc and A600-sc, normalized to their total spectral integral, are presented in Fig. 3.

The interest of this type of normalized TDS spectra is that they are independent of the ^2H surface concentration applied during the charging step [35]. This normalization makes thus possible the comparison between two experimental spectra even, if the value of $c_{0, \text{charging}}$ is not accurately known, as in the case in this work, or evolves from one experiment to each other, e. g. due to the aging of the charging solution [35]. This property of normalized spectra is also useful when comparing calculated and experimental TDS spectra in order to investigate the effect of D on the spectral shape, as is done in Sections [Diffusion coefficient derivation](#), [Diffusion coefficient validation](#) and [Diffusion in A600-sc: simulations using derived \$\{D_0, E_D\}\$](#) .

Some general remarks concerning the experimental A600-pc and A600-sc TDS spectra are listed below.

1. “Traditional” TDS spectra (Fig. 3a) for both polycrystalline and single crystal A600 are characterized by one intense desorption peak at approximately 395 K.
2. “Hybrid-294 K” TDS spectra (Fig. 3b) are characterized by a non negligible desorption flux at $t = 0$ which as aging progresses, weakens until it falls below the detection limit of the mass spectrometer. Then when a temperature ramp is applied ($\phi = 10 \text{ K min}^{-1}$ from $(294 \pm 2) \text{ K}$ to above 1273 K) a significant desorption peak occurs of approximately the same intensity ($4.2 \cdot 10^{-4} \text{ cm}^{-2} \text{ s}^{-1}$) for both the polycrystalline and single crystal model materials.
3. “Hybrid-409 K” TDS spectra (Fig. 3c) are characterized by an early desorption peak when the system reaches the elevated aging temperature ($(409 \pm 1) \text{ K}$). The signal then weakens as aging progresses before, like for “hybrid-294 K” testing, falling below the detection limit of the mass spectrometer. The second temperature ramp ($\phi = 10 \text{ K min}^{-1}$ from $(409 \pm 1) \text{ K}$ to above 1273 K) produces a second very noisy small desorption peak just above the

mass spectrometer detection limit, which is not visible in Fig. 3c.

No significant difference between experimental spectra recorded on both A600-pc and A600-sc samples can be highlighted in Fig. 3, even during aging at room temperature, which is supposed to enhance a possible grain boundary contribution [31]. These results hint that hydrogen transport processes are similar in these two materials and consequently that grain boundaries have no, or only a negligible, effect on hydrogen diffusion in A600 for the grain size and experimental conditions investigated.

Diffusion coefficient derivation

A “traditional” normalized TDS spectrum performed on A600-pc and its fit, using the numerical routine presented briefly in Section [Numerical analysis](#) (more details are available in Ref. [29]), are shown in Fig. 4. The numerical code was used to simultaneously adjust the pre-exponential constant (D_0) and activation energy (E_D) using literature diffusion coefficient parameters [27,28] (Table 3) as the initial guess input parameters. To perform this fit, the value of $c_{0, \text{charging}}$ has been arbitrarily fixed, as TDS spectra, normalized to their total spectral integral, are independent of this parameter [35]. There is an overall good reproduction of experimental spectrum intensity, peak width and form associated with the derived fit, although some slight differences can be remarked. This seems to be due (i) to the accuracy of experimental input parameters (e.g. the measured temperature ramp and/or sample dimensions) and/or (ii) the effect of residual heterogeneities (see Section [Polycrystalline A600](#)) and/or grain boundaries existing in the A600-pc, which are neglected in the chosen diffusion model. The derived values of D_0 and E_D , as well as the related errors estimated statistically on the basis of three experimental measurements, are given in Table 3.

These values are smaller than those reported in literature [27,28]. However, using literature diffusion parameters to simulate the experimental spectrum performed on A600-pc leads to a quite good reproduction of this spectrum, as it can be seen in Fig. 4. To verify if the difference between the values

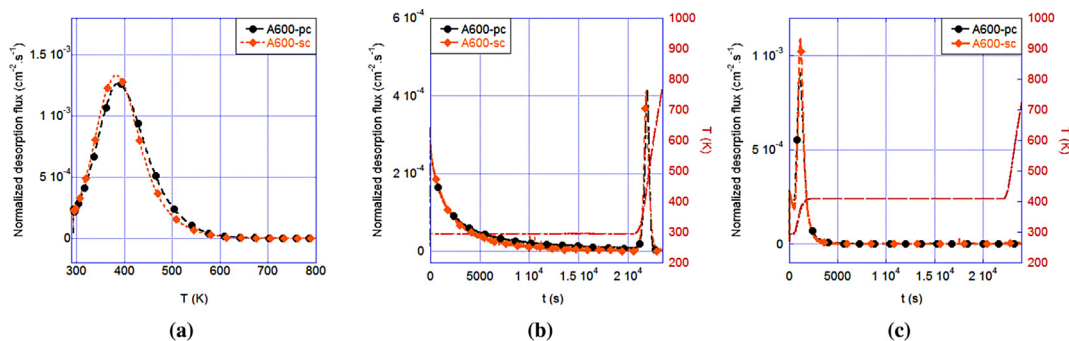


Fig. 3 – Normalized experimental (a) “traditional” and (b, c) “hybrid” TDS spectra for A600-pc and A600-sc. Two types of “hybrid” TDS spectra are displayed here: (b) “hybrid-294 K” which is subjected to an extended isotherm at $(294 \pm 2) \text{ K}$ and (c) “hybrid-409 K” which is subjected to an aging period at $(409 \pm 1) \text{ K}$ (Table 2). The red dashed lines in (b) and (c) show the evolution of temperature during the associated experiments. (For interpretation of the references to color in this figure legend, the reader is referred to the web version of this article.)

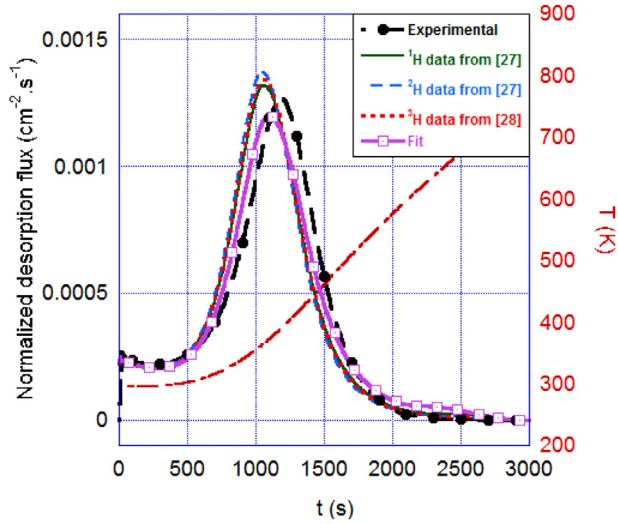


Fig. 4 – Experimental “traditional” TDS spectrum performed on ^2H pre-charged polycrystalline A600 and its best fit. Results are compared to simulated spectra based upon literature data for H, ^2H and ^3H (Table 3). The red dashed line shows the evolution of temperature during the associated experiment. (For interpretation of the references to color in this figure legend, the reader is referred to the web version of this article.)

measured in this study and those reported in the literature is significant and in the objective of validating the derived diffusion parameters measured, these different parameter sets were tested by simulating “hybrid” TDS spectra.

Diffusion coefficient validation

The aforementioned validation procedure was carried out by using the derived parameters to simulate a “hybrid-294 K” TDS spectra ($D_0 = 1.0 \cdot 10^{-2} \text{ cm}^2 \text{ s}^{-1}$ and $E_D = 45 \text{ kJ mol}^{-1}$). This simulation can be seen in Fig. 5 (and is referred to as ^2H data from this study in the figures) along with simulations using some literature diffusion coefficient parameters [27,28].

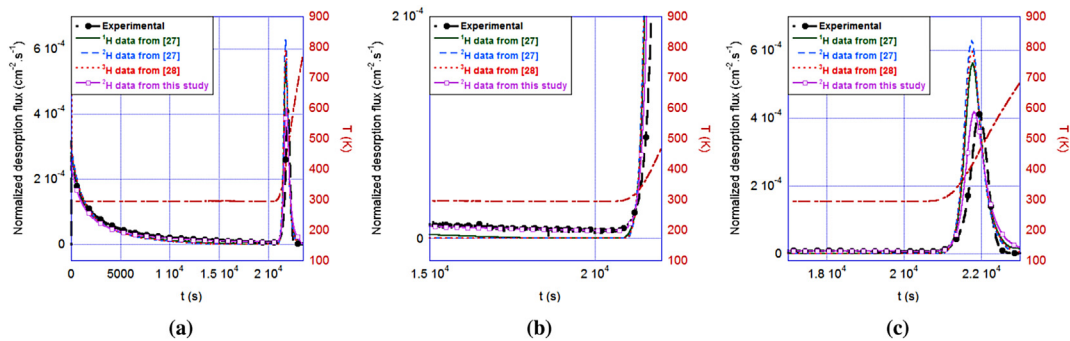


Fig. 5 – Experimental and simulated “hybrid 294 K” TDS desorption spectra for A600-pc. The diffusion parameters used for simulation can be seen in Table 3; (a) shows the entire “hybrid” spectra, (b) a zoom at the end of the isothermal period and (c) the non-isothermal TDS part of the spectra. The red dashed lines show the evolution of temperature during the associated experiments. (For interpretation of the references to color in this figure legend, the reader is referred to the web version of this article.)

All three simulated spectra reproduce well the beginning [isothermal] part of the experimental “hybrid” spectrum for an aging period of less than $1 \cdot 10^4 \text{ s}$. If a closer look is taken at the (i) isothermal part of the spectra for durations greater than $1 \cdot 10^4 \text{ s}$ and (ii) non-isothermal TDS spectra some clear discrepancies can be observed.

1. As the isothermal period continues (Fig. 5b) the improved efficiency of the simulation using the derived values is highlighted, as this spectrum mimics the [weak] intensity of the experimental spectrum, while the literature [27,28] simulated spectra quickly tend towards zero.
2. During the non-isothermal TDS analysis stage (Fig. 5c); both the intensity and placement of the desorption peak is much better reproduced using the derived diffusion coefficient parameters (“ ^2H data from this study”) as compared to those from the literature.

This relatively accurate simulation of an experimental TDS spectrum using diffusion coefficient parameters derived from another experimental spectrum (subjected to different experimental conditions) allows the $\{D_0, E_D\}$ combination obtained from the fitting method to be validated. Furthermore, this shows that the imposed system simplifications, such as the use of only Fick’s second law and the assumption that grain boundaries do not play a significant role as neither diffusion short-circuits or trap sites, see Section Numerical analysis, are applicable for this hydrogen-material system.

Diffusion in A600-sc: simulations using derived $\{D_0, E_D\}$

After the diffusion coefficient parameters for polycrystalline A600 have been validated, they were used to simulate “traditional” and “hybrid” TDS spectra for A600-sc.

Fig. 6a shows the “traditional” experimental and simulated spectra performed on A600-sc, see Table 2 for experimental conditions. There is an overall very good correlation between the simulated and experimental spectra, with a very good reproduction of the (i) low temperature normalized desorption intensity and spectral form, (ii) the temperature of maximum desorption and (iii) general peak form. From this first

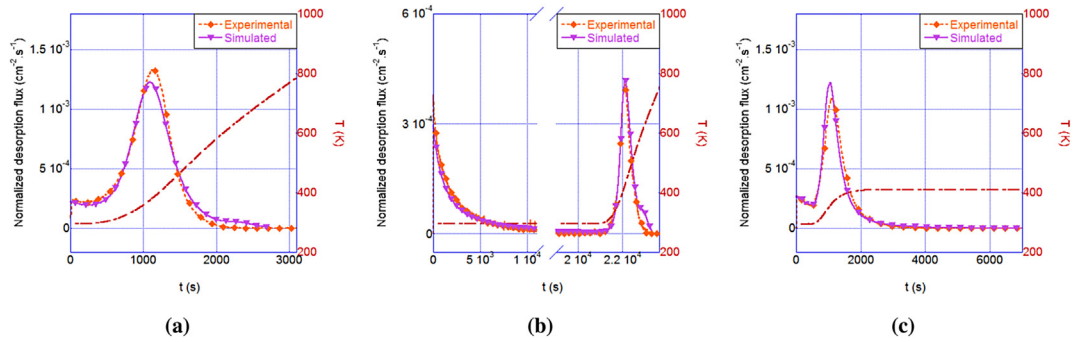


Fig. 6 – Normalized experimental and simulated (a) “traditional”, (b) “hybrid-294 K” and (c) “hybrid-409 K” TDS spectra (Table 2) for A600-sc. Simulations were carried out using the derived and validated diffusion coefficient $\{D_0, E_D\}$ combination for A600-pc, see Table 3. The red dashed lines show the evolution of temperature during the associated experiments. (For interpretation of the references to color in this figure legend, the reader is referred to the web version of this article.)

simulation, it would seem as though the derived $\{D_0, E_D\}$ pair from A600-pc adequately describe the diffusion interactions taking place in the single crystal of A600-like alloy.

Next, the $\{D_0, E_D\}$ pair was used to simulate the low temperature (294 K) “hybrid” TDS spectra using all sample history parameters. The results were compared to their experimental counterparts for A600-sc, see Fig. 6b. This simulation reproduces very well the normalized desorption spectra during both the room temperature isotherm ($t \leq 2.1 \cdot 10^4$ s) and “traditional” TDS type analysis ($t \geq 2.1 \cdot 10^4$ s and $\phi = 10$ K min)⁻¹. This is extremely evident at low temperature ($T = 294 \pm 2$ K, $t \leq 2.1 \cdot 10^4$ s), where grain boundary diffusion is often considered to be a major contribution [19,20,16,31].

As an overall very good correlation has been achieved for the previous simulations, one last comparison can be done. An experimental “hybrid” TDS spectra, having been aged for 6 h at 409 K was simulated. This aging temperature (409 ± 1 K) is very interesting as it approaches the temperature range at which volume diffusion is often considered the major contribution [31] but grain boundaries could still play a short-circuit or trapping role in deuterium diffusion. This comparison can be seen in Fig. 6c. In agreement with the previous remarks, the reported spectrum is well reproduced by the derived values seen in Table 3.

The comparison of experimental A600-sc TDS spectra, with their simulated counterparts using the $\{D_0, E_D\}$ combination derived from A600-pc spectra, seems to confirm that grain boundaries have no significant effect on the diffusion of ^2H in A600, for the grain size and experimental conditions investigated. Moreover, these results demonstrate that the values of D_0 and E_D , determined in this work, are representative of an interstitial diffusion mechanism.

Conclusion

The goal of this article was to address the role grain boundaries may play on the diffusion of deuterium in nickel base alloy 600. To study this phenomenon, two model materials were used: (i) a polycrystalline A600 (after a large majority of dislocations and precipitates have been eliminated) and (ii) an A600-like single crystal. Experimental comparisons of “traditional”, “hybrid-

294 K” and “hybrid-409 K” TDS spectra highlighted some clear similarities in the experimental results obtained on the A600-pc and A600-sc materials, leading to the conclusion that grain boundaries do not play a significant role in H transport in A600, for the grain size and experimental conditions investigated.

This study has been carried out in the framework of better understanding the interactions taking place between H and industrial A600, used as the main component of the steam generator tubes of PWR nuclear power plants. It would then be important to also study the interactions taking place at the other types of sites, intrinsically present in the industrial material, for example chromium carbides, dislocations and vacancies. This study on the influence of grain boundaries on the diffusion of hydrogen in nickel base alloy 600 serves as a first step towards the understanding of more complicated H-material interaction systems. The obtained results concerning the diffusion of ^2H in this alloy could serve as input data for more in-depth analysis of interactions between H and crystallographic heterogeneities (i.e. vacancies, dislocations, carbides, etc.) in A600 as suggested in Ref. [29].

Acknowledgments

The authors would like to thank EDF for their financial support and M.C. Lafont (CIRIMAT, ENSIACET) and S. Poissonnet (CEA/DEN/DANS/DMN/SRMP) for their help with material observations and analyses.

REFERENCES

- [1] Coriou H, Grall L, Le Gall Y, Vettier S. Corrosion fissurante sous contrainte de l'inconel dans l'eau à haute température, Stress corrosion cracking of Inconel in high temperature water, 3ème Colloque Annuel de Métallurgie, 1960.
- [2] Rebak R, Szklarska-Smialowska Z. The mechanism of stress corrosion cracking of alloy 600 in high temperature water. *Corr Sci* 1996;38(6):971–88.
- [3] Economy G, Jacko R, Pement F. IGSCC behavior of alloy 600 steam generator tubing in water or steam tests above 360° C. *Natl Asso Corr Eng* 1987;43(12):727–34.

-
- [4] Totsuka N, Szklarska-Smialowska Z. Effect of electrode potential on the hydrogen-induced IGSCC of alloy 600 in an aqueous solution at 350° C. *Corrosion* 1987;43:734–8.
- [5] G. Was, D. Paraventi, J. Hertzberg, Mechanisms of environmentally enhanced deformation and intergranular cracking of Ni–16Cr–9Fe alloys, *EUROCORR '96*, EFC by the Institut of materials, 410–420.
- [6] Symons D. The effect of hydrogen on the fracture toughness of alloy X-750 at elevated temperatures. *J Nucl Mater* 1999;265:225–31.
- [7] Chêne J, Brass A-M. Role of temperature and strain rate on the hydrogen-induced intergranular rupture in alloy 600. *Metall Mater Trans A* 2004;35A:457–64.
- [8] Jambon F, Marchetti L, Jomard F, Chêne J. Mechanism of hydrogen absorption during the exposure of alloy 600-like single-crystals to PWR primary simulated media. *J Nucl Mater* 2011;414(3):386–92.
- [9] Molander A, Norring K, Andersson P, Elfsing P. Environmental effects on PWSCC initiation and propagation in alloy 600. In: Busby J, Ilevbare G, Andresen P, editors. 15th International Conference on environmental degradation of materials in nuclear power systems – water reactors. John Wiley & Sons; 2011. p. 1699–711.
- [10] Jambon F, Marchetti L, Jomard F, Chêne J. Characterization of oxygen and hydrogen migration through oxide scales formed on nickel-base alloys in PWR primary medium conditions. *Solid State Ionics* 2013;231:69–73.
- [11] A. Troiano, The role of hydrogen and other interstitials in the mechanical behavior of metals. *Trans ASM*;52(1690):54–80.
- [12] Matsumoto T, Eastman J, Birnbaum H. Direct observations of enhanced dislocation mobility due to hydrogen. *Scr Metall* 1981;15:1033–7.
- [13] Birnbaum H. Hydrogen effects in metals, TSM. Warrendale, PA: USA; 1990.
- [14] Young G, Scully J. Evidence that carbide precipitation produces hydrogen traps in Ni-17Cr-8Fe alloys. *Scr Mater* 1997;36(6):713–9.
- [15] Symons D, Young GA, Scully J. The effect of strain on the trapping of hydrogen at grain-boundary carbides in Ni-Cr-Fe alloys. *Metall Mater Trans A* 2001;32:369–78.
- [16] Louthan MR, Donovan J, Caskey GJ. Hydrogen diffusion and trapping in nickel. *Acta Metall* 1975;23:745–9.
- [17] Harris T. Hydrogen diffusion and trapping in electrodeposited nickel. Ph.D. thesis. Massachusetts Institute of Technology; 1979.
- [18] Harris T, Latanision R. Grain boundary diffusion of hydrogen in nickel. *Metall Trans A* 1991;22:351–5.
- [19] Chanfreau A. Etude de la précipitation de l'hélium 3 dans un acier inoxydable 316L; Influence sur la diffusion de l'hydrogène. Ph.D. thesis. University de Paris-Sud Centre d'Orsay; 1992.
- [20] Brass A-M, Chanfreau A. Accelerated diffusion of hydrogen along grain boundaries in nickel. *Acta Mater* 1996;44(9):3823–31.
- [21] Oudriss A, Creus J, Bouhattate J, Conforto E, Berziou C, Savall C, et al. Grain size and grain-boundary effects on diffusion and trapping of hydrogen in pure nickel. *Acta Mater* 2012;60(19):6814–28.
- [22] Dieudonné T, Marchetti L, Jomard F, Wery M, Chêne J, Allely C, et al. SIMS analysis of deuterium absorption and diffusion in austenitic Fe-Mn-C steels. *Defect Diffus Forum* 2012;323–325:477–83.
- [23] Yao J, Cahoon J. Experimental studies of grain boundary diffusion of hydrogen in metals. *Acta Metall* 1991;39(1):119–26.
- [24] Ono K, Meshii M. Hydrogen detrapping from grain boundaries and dislocations in high purity iron. *Acta Metall* 1992;40(6):1357–64.
- [25] Oudriss A, Creus J, Bouhattate J, Savall C, Peraudeau B, Feaugas X. The diffusion and trapping of hydrogen along the grain boundaries in polycrystalline nickel. *Scr Mater* 2012;66(1):37–40.
- [26] Di Stefano D, Mrovec M, Elsässer C. First-principles investigation of hydrogen trapping and diffusion at grain boundaries in nickel. *Acta Mater* 2015;98:306–12.
- [27] Rota E, Waelbroeck P, Wienhold P, Winter J. Measurements of surface and bulk properties for the interaction of hydrogen with Inconel 600. *J Nucl Mater* 1982;111–112:233–9.
- [28] Sakamoto K, Sugisaki M. Diffusion coefficient of tritium in Ni-based alloy. *Fusion Sci Technol* 2002;41:912–4.
- [29] Hurley C, Martin F, Marchetti L, Chêne J, Blanc C, Andrieu E. Numerical modeling of thermal desorption mass spectroscopy (TDS) for the study of hydrogen diffusion and trapping interactions in metals. *Int J Hydrogen Energy* 2015;40(8):3402–14.
- [30] Lecoester F, Chêne J, Noel D. Hydrogen embrittlement of the Ni-base alloy 600 correlated with hydrogen transport by dislocations. *Mater. Sci Eng, A* 1999;262:173–83.
- [31] Harrison L. Influence of dislocations on diffusion kinetics in solids with particular difference to the alkali halides. *Trans Faraday Soc* 1961;57:1191–8.
- [32] Whipple R. Concentration contours in grain boundary diffusion. *Phil Mag* 1954;45:1225–36.
- [33] Mishin Y, Herzig C, Bernardini J, Gust W. Grain boundary diffusion: fundamentals to recent developments. *Int Mat Rev* 1997;42(4):155–77.
- [34] McNabb A, Foster P. A new analysis of the diffusion of hydrogen in iron and ferritic steels. *Trans Metall Soc AIME* 1963;227:618–27.
- [35] Hurley C. Kinetic study of hydrogen-material interactions in nickel base alloy 600 and stainless steel 316l through coupled experimental and numerical analysis. Ph.D. thesis. Université de Toulouse, Institut National Polytechnique de Toulouse; 2015.
- [36] Scipy library and documentation on included packages. <http://scipy.org/>; [accessed 17.09.15].